2nd URSI AT-RASC, Gran Canaria, 28 May – 1 June 2018

Conjuring Radar Meteor Head-Echoes

J. D. Mathews[(1)]
(1) The Pennsylvania State Un., University Park, PA USA

Abstract

The argument surrounding under-dense vs. over-dense radar meteors has raged for decades. Here we consider the head-echo case by the noting that the two limiting scattering regimes for the same radar (scattering) cross-section (RCS) are each easily described. We give a synopsis of scattering from a perfectly conducting (PC) sphere that represents the manifestly over-dense limit. We contrast this with coherent (in-phase) scattering from an ensemble of N electrons all located within a ~1/4-wavelength diameter volume containing the meteoroid. Note that N is the *absolute minimum* number of electrons yielding a given RCS and that the continuum of equal RCS electron distributions leading to the PC-sphere all require more electrons and thus higher energy to assemble. Here we find the loci of equal RCS for these two limiting cases at three wavelengths—70 cm, 1.29 m, and 6 m—corresponding to the Arecibo Observatory (AO), EISCAT_3D, and Jicamarca Radio Observatory (JRO) radars, respectively. We also plot on each of these curves the location of a single-pulse (unaveraged), 100 km range, SNR=1 event. In all cases the over-dense (Rayleigh scatter) meteor would correspond to an improbably large object while the number of electrons, N, yielding the same RCS is reasonable. Invoking Occam's Razor, we conclude that the vast majority of head-echo radar meteors are under-dense. This conclusion is important to many aspects of meteoroid physics including mass flux determinations as N is relatively easy to link to meteoroid physics and thus to meteoroid mass. This remains largely true when meteoroid inhomogeneity and fragmentation are considered.

1. Introduction

Theory and observation each inform the other. Here we attempt to examine the radar meteor head-echo "origins" assumptions by considering the limiting cases and by emphasizing the continuum of largely indistinguishable possibilities between these limits. We relate these results to theoretical modeling of plasma production by an ablating meteoroid and FDTD solutions for the RCS of the resultant over-dense head-echoing region [1-4]. Immediate assumptions in these modeling results include symmetry (except for B-field effects) of the plasma along the trajectory axis of the meteoroid and that the extent of the head-echo plasma surrounding the meteoroid is of order of the local atmospheric mean free path (MFP). Also, the meteoroid is taken to be a single homogenous solid (or melt) that simply ablates. That is, fragmentation is necessarily excluded from consideration.

The only information we have from single frequency radar is the meteor head-echo RCS (which is very difficult to measure on an absolute basis) and delay-Doppler information along with any pointing information that locates the event on the sky. Here we, in essence, reverse engineer this limited knowledge to determine what other information, if any, can be gleaned from these events. For now, we assume that the radar meteor head-echo is slowly varying from pulse-to-pulse and that it exhibits no intra-pulse structure that would point to fragmentation [5-8]. We further assume that the underdense head-echo derives from Coherent Scattering from N electrons (CSN limit) in the immediate vicinity of the meteoroid and that are traveling with the meteoroid. At the other limit we consider Rayleigh (overdense) scattering from the surface electrons in the solid (perfectly conducting) meteoroid body. We consider the implications of both limits, and the continuum of indistinguishable intermediate states, *all of which produce the same RCS*. We arrive at the conclusion that the CSN limit is the most likely explanation for observed head-echoes [9, 10].

Note that the above head-echo scenario parallels that of a classical under-dense meteor trail where the net RCS is derived from coherent scattering, over about two Fresnel zones, from the train of equally-illuminated electrons [10]. Also note that as the spatial distribution of electrons widens to many wavelengths in three-dimensions, interference effects become dominant with ionospheric incoherent scattering, exhibiting very small bulk RCS, as one outcome. The absence of a trail-echo for most head-echo events is another outcome.

We begin by reviewing the radar (back) scattering cross-sections from both a PC-sphere and in the CSN limit (Sections 2 & 3). In Section 4 we concisely derive the simplest monostatic radar equation. In Section 5 we directly compare the number of coherently scattering electrons yielding the same RCS as a PC-sphere as we vary sphere radius. We also directly compare the implied parameters of radar meteor head-echo events observed at 100 km range by the AO, JRO, and EISCAT_3D radars. This is followed by the Discussion and the Conclusions.

2. Scattering from a PC Sphere

Consider a perfectly conducting sphere of radius a<<λ=radar wavelength. Then the Rayleigh backscatter (monostatic) radar scattering cross-section (RCS=σ_{bs}; m^2) is (see Section 11.8 of Balanis [11])

$$\sigma_{BS} = \frac{9\lambda^2}{4\pi}\left(\frac{2\pi a}{\lambda}\right)^6 \quad (1)$$

Eqn (1) approximates the LHS of the Figure 1 full-analytic-solution plot—parameter definitions are given in the Fig. 1 caption. The full-range RCS for a PC sphere is given in Balanis and elsewhere.

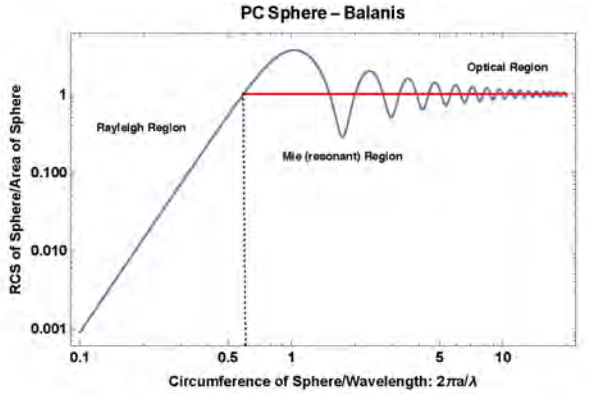

Figure 1. Normalized Radar scattering Cross-Section (RCS) of a perfectly conducting (PC) sphere in the Rayleigh, Mie, and optical regions where a=radius of sphere & λ=probing wavelength. The red line approximates both the Mie and optical regions above the first normalized RCS = 1 point which occurs at 2πa/λ=0.592724. The full range analytic solution is given by Balanis [11] eqn. 11-247.

The Mie/optical scattering case for which normalized-RCS≃1 (it oscillates about 1; see Figure 1) occurs over 2πa/λ≥0.592724 in the full analytic solution. For this case, in comparing coherent scattering from N electrons with scattering from the PC sphere, we find simply that

$$\sigma_{BS} \simeq \pi a^2 \simeq 4\pi r_e^2 N^2 \quad (2)$$

3. Electron Ensemble Coherent Scattering

Next we consider Coherent back-Scattering from an ensemble of N electrons (CSN) all located within a ~1/4-wavelength diameter volume. This is the full "under-dense" case with all electrons equally illuminated. This assumption is readily tested. *Note that this is the most "efficient" scattering case in that the minimum number of electrons (in an underdense configuration) yields a given RCS.* The backscattering cross-section of a single electron is [12]

$$\sigma_{BS} = 4\pi r_e^2 \quad (3)$$

where r_e= classical electron radius ($2.8179403267\times10^{-15}$ m). If all electrons backscatter in phase (the scattered E-fields add) then the total backscatter (power) cross-section is

$$\sigma_{BS} = 4\pi r_e^2 N^2 \quad (4)$$

where no shadowing is considered [9,10].

4. The Monostatic Radar Equation

For transmitter power (Watts) P_T, gain G in the target direction, and range r, the Poynting flux magnitude is

$$\left|S(r)\right| = \frac{P_T G}{4\pi r^2} \quad (5)$$

The total backscatter Poynting flux at the receiver is

$$\left|S_R(r)\right| = \frac{P_T G}{4\pi r^2} \times \frac{\sigma_{BS}}{4\pi r^2} \quad (6)$$

The received power, assuming an impedance matched system, is $\left|S_R(r)\right| \times A_{eff}$ where effective area is $A_{eff} = \lambda^2 G / 4\pi$. Thus received power is

$$P_R = \frac{\lambda^2}{4\pi}\frac{P_T G^2}{(4\pi r^2)^2}\sigma_{BS} \quad (7)$$

Assuming thermal noise only, the receiver noise level is

$$P_N = k_B T_{sys} BW \quad (8)$$

where k_B = Boltzmann's constant, T_{sys} = system temperature, and BW is the sampled receiver noise bandwidth. Thus the signal-to-noise ratio is

$$SNR = P_R / P_N \quad (9)$$

5. Underdense vs. Overdense Scattering

In Figure 2 we plot the locus of equal RCS (σ_{bs}) for three radar wavelengths corresponding to AO, JRO, and EISCAT_3D. For this, we plot PC sphere radius (m) versus the number of coherent scattering electrons yielding the same RCS. That is, we find N by setting equations (1) and (4) equal until 2πa/λ≥0.592724 is reached at which point we use equation (2). The equation (2) transition from Rayleigh to Mie/optical RCS is seen in the slope changes in the Figure 2 curves. We note again that the two limits expressed in Figure 2 bound a continuum of indistinguishable intermediate results. If meteoroid inhomogeneity and fragmentation are included, the possible electron distributions yielding the same instantaneous RCS is uncountably larger. Notice that relatively few CSN electrons produce the same RCS as a relatively large, in terms of meteoroid size, PC-sphere.

Next we explore the implications of the Figure 2 results with respect to the approximate minimum meteor event detectable using the AO, JRO, and EISCAT_3D radars. This comparison will also serve to inform the community on the relative sensitivities of these HPLA radars.

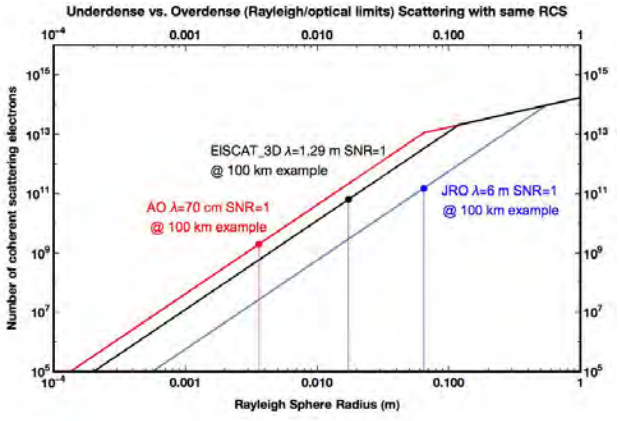

Figure 2. Here we show, at the three wavelengths corresponding to AO, JRO, and the new EISCAT_3D radars, the locus of equal RCS (σ_{bs}) for a perfectly conducting (PC/over-dense) sphere (radius a) versus the number (N) of coherently (under-dense) scattering electrons that yield the same RCS as the PC sphere. Also shown for radar comparison purposes are the 100 km SNR=1 RCS results for the three radars. For this, we used 1 MHz BW, 1 MW transmitter power, and 100 K system temperatures for AO & EISCAT_3D and 5000 K for JRO. On the log-log scale, changes in these parameters move the SNR=1 points only a small distance along the respective loci. The wavelength and the antenna gain are the dominant features in these results. The change of slope in the above curves is due to the transition of Rayleigh scattering (LHS) to Mie/Optical scattering (RHS).

To accomplish this comparison, we use equations (7), (8), & (9) to illustrate an unaveraged (single pulse), SNR=1 event at 100 km range observed by each radar. For this we assume 1 MHz bandwidth (BW) and 1 MW transmitter power for all three systems. The AO & EISCAT_3D system temperature is assumed to be 100 K while 5000 K is assumed for JRO. The three results below are plotted on the respective Figure 2 curves.

AO: The AO 430 MHz (0.6972 meters wavelength) radar system has an SNR=1 for a 3.6 mm radius PC-sphere at 100 km range for 1 MW transmitted and a system temperature of 100 K on a 1 MHz BW. We assume 61 dBi gain for AO. This is big particle. This RCS also corresponds to $N=1.886\times10^{9}$ electrons coherently scattering. If N is uniformly distributed into a λ/8 radius sphere, the resultant plasma frequency is 7.4 MHz.

JRO: The JRO 50 MHz radar system has an SNR=1 for a 6.426 cm radius sphere at 100 km range for 1 MW transmitted and a system temperature of 5000 K on a 1 MHz BW. We assume 41 dBi gain to average over array configurations. The PC-sphere result is a BIG particle—major space debris size. In practice, JRO system temperature varies from 4000 - 40,000 K depending on the galaxy (Marco Milla, private communication, 9 June 14). JRO full-array antenna gain is ~44 dBi with quarter array gain of ~38 dBi, and individual module gain of ~26 dBi. Using full-array gain, JRO sees just $N=1.551\times10^{11}$ electrons with SNR=1 at 100 km range. If N is uniformly distributed into a λ/8 radius sphere, the resultant plasma frequency is 2.7 MHz.

EISCAT_3D: EISCAT_3D will operate at 233 MHz (1.287 m wavelength) and 5 MW transmit power—we use 1 MW here—with 43 dBi transmit/receive gain and a typical system temperature of 100 K. EISCAT_3D will ultimately include three identical receive stations; we consider only the monostatic case here. Under these parameters the SNR=1 instantaneous detection of a 100 km event is a 0.0172 meter radius PC-sphere or $N=6.45\times10^{11}$ electrons coherently scattering. If N is uniformly distributed into a λ/8 radius sphere, the resultant plasma frequency is 17.3 MHz.

6. Discussion

Recently radar meteor head-echo issues were examined using FDTD solutions to the Maxwell equations in the presence of plasma modeled via various electron (plasma frequency) distributions to find corresponding backscatter RCS values [1,4]. In this Marshall et al. [4] note that the head-echoing plasma distribution likely scales according to the local atmospheric mean-free-path (MFP). This conclusion is supported by Dimant & Oppenheim [2,3] who model the formation of the primary ablated particle region around the meteoroid and find, via a kinetic theory description of primary particle distribution and subsequent collisions with atmospheric molecules, the resultant ionization distribution. Both [3,4] note that the largest head-echo regions would form at the highest altitudes but that it is "improbable that a meteoroid could form a large, dense head echo (plasma) in the atmosphere" in this situation [1]. However, High-Altitude Radar Meteors (HARM) have been reported [13-15]. Note that HARMs, attributed to sputtering, produce an interesting situation where onset of the minimal ionization traveling with the meteoroid is contrasted with the size of the meteoroid needed to produce the same detectable RCS. This supports our primary contention that CSN (Coherent Scattering from N electrons) is likely the dominant source of the radar head-echo.

7. Conclusions

In comparing under- vs. over-dense meteor head-echo "formation" we find that the over-dense (Rayleigh scatter) meteor would correspond to an improbably large object (except for bolides) while the number of electrons, N, yielding the same RCS is reasonable. Invoking Occam's Razor, we conclude that the vast majority of head-echo radar meteors are under-dense. We further note that meteoroid inhomogeneity and fragmentation completely muddle attempts to model head-echo formation. In particular, any conclusion that the head-echo RCS is linked to mass is tenuous at best unless (underdense) CSN is true. That is, CSN does seem to relate RCS to meteoroid mass with fewer assumptions. The existence of

High-Altitude Radar Meteors [13, 14, 15] seems to confirm this viewpoint. This conclusion is important to many aspects of meteoroid physics, not least, mass flux determinations.

Finally, it is important to emphasize that at constant RCS the CSN and PC-sphere head-echoes are indistinguishable from each other and from the continuum of intermediate states. Additionally the statement that, "Only a small volume of the dense plasma sufficiently close to the meteoroid contributes to the corresponding radar wave reflection." [2], is not the case. All illuminated electrons contribute to the head-echo including those in the forming trail [10]. However scattering from those electrons outside of $\lambda/8$ radius tend to add incoherently (this is not traditional incoherent scattering). It does seem likely that a carefully calibrated EISCAT_3D can confirm, or deny, a link between head-echo RCS and meteoroid mass especially when following HARM events into the traditional meteor zone—corresponding optical meteor information would be most helpful too. In these studies, the transition between wavelength-dominated and MFP-dominated head-echo volume may statistically appear.

8. Acknowledgements

This effort was supported under NSF Grants ATM 07-21613 and AGS 12-02019 to The Pennsylvania State University. Our Mathematica notebook for all aspects of this paper will be supplied on request.

9. References

1. Marshall, R. A., and S. Close (2015), "An FDTD model of scattering from meteor head plasma", J. Geophys. Res. Space Phys., **120**, pp. 5931-5942, doi: 10.1002/2015JA021238.

2. Dimant, Y. S., and M. M. Oppenheim (2017), "Formation of plasma around a small meteoroid: 1. Kinetic theory", J. Geophys. Res. Space Phys., **122**, pp. 4669-4696, doi: 10.1002/2017JA023960.

3. Dimant, Y. S., and M. M. Oppenheim (2017), "Formation of plasma around a small meteoroid: 2. Implications for radar head echo", J. Geophys. Res. Space Phys., **122**, pp. 4697-4711, doi: 10.1002/2017JA023963.

4. Marshall, R. A., P. Brown, and S. Close (2017), "Plasma distributions in meteor head echoes and implications for radar cross section interpretation", Planet. Space Sci., **143**, pp. 203-208, doi: 10.1016/j.pss.2016.12.011.

5. Roy, A., S. J. Briczinski, J. F. Doherty, and J. D. Mathews (2009), "Genetic-algorithm-based parameter estimation technique for fragmenting radar meteor head-echoes", IEEE Geosci. Remote Sens. Lett., **6(3)**, pp. 363-367, doi: 10.1109/LGRS.2009.2013878.

6. Mathews, J. D., S. J. Briczinski, A. Malhotra, and J. Cross (2010), "Extensive meteoroid fragmentation in V/UHF radar meteor observations at Arecibo Observatory", Geophys. Res. Lett., **37**, L04103, doi: 10.1029/2009GL041967.

7. Malhotra, A., and J. D. Mathews (2011), "A statistical study of meteoroid fragmentation and differential ablation using the Resolute Bay incoherent scatter radar", J. Geophys. Res., **116**, A04316, doi: 10.1029/2010JA016135.

8. Zhu, Q., R. Dinsmore, B. Gao, and J. D. Mathews (2016), "High-resolution radar observations of meteoroid fragmentation and flaring at the Jicamarca Radio Observatory", Mon. Not. R. Astron. Soc., **457**, pp. 1759-1769, doi: 10.1093/mnras/stw070.

9. Mathews, J. D., D. D. Meisel, K. P. Hunter, V. S. Getman, and Q. Zhou (1997), "Very high resolution studies of micrometeors using the Arecibo 430 MHz radar", Icarus, **126**, pp. 157-169, doi: 10.1006/icar.1996.5641.

10. Mathews, J. D. (2004), "Radio science issues surrounding HF/VHF/UHF radar meteor studies", J. Atmos. Solar-Terr. Phys., **66#3**, pp. 285-299, doi: 10.1016/j.jastp.2003.11.001.

11. Balanis, C. A. (1989), "Advanced Engineering Electromagnetics", 1st ed., 981 pp., John Wiley and Sons, New York.

12. Bekefi, G. (1966), Radiation Processes in Plasmas, 364 pp., Wiley, New York.

13 Gao, B., and J. D. Mathews (2015), High-altitude meteors and meteoroid fragmentation observed at the Jicamarca Radio Observatory, Mon. Not. R. Astron. Soc., 446, pp. 3404-3415, doi: 10.1093/mnras/stu2176.

14. Gao, B., and J. D. Mathews (2015), High-altitude radar meteors observed at Jicamarca Radio Observatory using a multi-baseline interferometric technique, Mon. Not. R. Astron. Soc., 452, pp. 4252-4262, doi: 10.1093/mnras/stv1548.

15. Mathews, J. D., B. Gao, S. Kesaraju, and S. Raizada (2017), Meteoroid Sputtering, High-Altitude Radar and Optical Meteors, and Sources for Lower-Thermospheric Metals, Proceedings of the 32nd URSI General Assembly and Scientific Symposium, Montréal, Canada, Paper GH27-24.